RSC Advances

PAPER

View Article Online
View Journal | View Issue

Cite this: *RSC Adv.*, 2023, **13**, 34455

Preparation of barium sulfate chelating agent DTPA-5Na and molecular dynamics simulation of chelating mechanism

Chao Ma,*[abc] Xin Liu, *[a] Cheng Wang,[a] Shengtian Gao[a] and Xiaoyi Huang[a]

Barium sulfate ($BaSO_4$) scale is dense and hard, making it difficult to remove using conventional acid and alkali treatments. Diethylenetriaminepentaacetic acid (DTPA) and its complexes have been identified as important chelating agents for the removal of $BaSO_4$ scale. However, DTPA has good solubility only under strong alkali conditions, which in turn exacerbate scaling. To improve the solubility and chelation effectiveness of DTPA, penta sodium diethylenetriamine-pentaacetate (DTPA-5Na) was synthesized using chloroacetic acid, diethylenetriamine, sodium carbonate, and sodium hydroxide as raw materials. The structure of DTPA-5Na was characterized by infrared spectroscopy and ^{1}H-NMR, and its chelation effectiveness was evaluated. Experimentation demonstrated that under conditions of 50 °C and with a molar ratio of chloroacetic acid ($ClCH_2COOH$), sodium carbonate (Na_2CO_3), sodium hydroxide (NaOH), and diethylenetriamine (DETA) of 5.00 : 2.50 : 5.25 : 1.00, the reaction for 6 hours resulted in the optimal chelation value of DTPA-5Na at 76.8 mg $CaCO_3$·per g. Analysis of the chelation and dissolution of $BaSO_4$ scale using DTPA-5Na and microstructural scanning electron microscopy of the $BaSO_4$ crystal indicate that DTPA-5Na functions through solubilization, lattice distortion, and flaking dispersion to remove $BaSO_4$. Molecular dynamics simulation software was used to simulate the chelation mechanism of DTPA-5Na, where the results indicated strong adsorption of DTPA-5Na to the surface of $BaSO_4$. The adsorption energy follows the order of (120) surface > (001) surface > (100) surface > (210) surface. The adsorption is mainly a result of the interaction between the carboxylic "O" atom in DTPA-5Na and the (001), (100), and (120) surfaces of $BaSO_4$ scale, while N atoms in DTPA-5Na structure primarily interact with the (210) surface. The adsorption of "O" atoms is stronger than that of "N" atoms in the DTPA-5Na structure.

Received 16th August 2023
Accepted 7th November 2023

DOI: 10.1039/d3ra05564g

rsc.li/rsc-advances

1 Introduction

During oilfield production, the injection of water that is incompatible with the formation water or the existence of reservoirs with high levels of SO_4^{2-} and Ba^{2+},[1–5] and even the introduction of $BaSO_4$ weighting material into the reservoir during drilling operations,[6–8] can all generate varying degrees of $BaSO_4$ scaling. $BaSO_4$ scale possesses stable physicochemical properties, including hardness, crystalline density, and strong adhesion, resulting in its adsorption and deposition in the reservoir, wellbore, and pipelines, leading to reservoir contamination and pipeline constriction. Due to the low solubility of $BaSO_4$ in water and its difficulty in dissolution in common acid/base solutions, chelating agents are commonly used for removal.[9–12] Currently used chelating agents include hydroxycarboxylic acid salts, organophosphorus acid salts, amino carboxylic acid salts, macrocyclic polyethers, polyamines, *etc.* Among these, the amino carboxylic acid salt diethylenetriaminepentaacetic acid (DTPA) exhibits strong chelating ability for heavy metals such as barium and strontium; it wets, disperses, and breaks apart hard scale, transforming it into loose particles for further removal.[13,14] Research shows that the chelating ability of DTPA is mainly due to the involvement of COO^- groups in DTPA, which can only be smoothly dissociated in a strong alkaline environment, exhibiting excellent chelating ability. However, COO^- groups are difficult to dissociate under acidic, neutral, and weakly alkaline conditions, severely limiting their chelating performance. DTPA-5Na is an amino carboxylic acid salt chelating agent that exhibits similar chelating ability to DTPA and has easily dissociable COO^- groups. Therefore, the synthesis of a DTPA-5Na salt with good solubility and suitability for a wider range of acid/base environments has significant significance for the chelation removal of $BaSO_4$.

[a]*School of Petroleum Engineering, Yangtze University, Wuhan 434100, China. E-mail: 500526@yangtzeu.edu.cn*

[b]*Key Laboratory of Oil and Gas Drilling and Production Engineering, Wuhan 434100, China*

[c]*National Engineering Research Center for Oil & Gas Drilling and Completion Technology, Wuhan 434100, China*

There are two main methods for synthesizing DTPA-5Na, namely, the sodium cyanide method and the chloroacetic acid method.[15] The former involves the use of sodium cyanide, formaldehyde, and diethylenetriamine as raw materials, but its reliance on the highly toxic cyanide and difficulties in controlling and managing its production have caused it to be discarded. Instead, the latter method utilizes chloroacetic acid ($ClCH_2COOH$), diethylenetriamine (DETA), sodium hydroxide (NaOH), or sodium carbonate (Na_2CO_3) to synthesize DTPA-5Na, which has raw materials that are readily available and a relatively simple process, making it a commonly used method in laboratories for the preparation of DTPA-5Na. For example, Lin *et al.*[16] monitored and regulated the pH during the synthesis process to stabilize it between 11 to 11.5, DTPA-5Na was prepared by keeping the reaction mixture at 30 °C for 1 hour, and the chelation value was measured to be between 40 to 50 mg $CaCO_3$·per g. Similarly, Wang *et al.*[17] stabilized the pH at 11.5 during the synthesis process and prepared DTPA-5Na by keeping the reaction mixture at 50 °C for 1 hour, the chelation value was measured to be ≥ 60 mg $CaCO_3$ per·g. Xu *et al.*[18] also stabilized the pH at 11.5 during the synthesis process and prepared DTPA-5Na by keeping the reaction mixture at 45 °C for 8 hours, the chelation value was measured to be 71.04 mg $CaCO_3$·per g. Therefore, the chelation value of DTPA-5Na is closely related to its synthetic conditions. In this study, we drew inspiration from the chloroacetic acid method and used diethylenetriamine, chloroacetic acid, sodium carbonate, and sodium hydroxide as raw materials to improve the synthesis conditions and enhance the chelation performance of DTPA-5Na. We analyzed the dissolution phenomena of barium sulfate scale and the microscopic changes of barium sulfate scale crystals before and after chelation. Furthermore, we used Materials Studio 5.0 molecular simulation software to simulate the scale removal mechanism of DTPA-5Na from a molecular dynamics perspective,[19] these studies provide an effective approach for the development and design of barium sulfate scale chelating agents.

2 Materials and methods

2.1 Materials

Anhydrous sodium hydrogen carbonate, chloroacetic acid, sodium hydroxide, and diethylenetriamine were obtained in high purity (99.9%) from Shanghai Maclin Biochemical Technology Co., Ltd. Anhydrous ethanol was purchased from Tianjin Bohua TONG Chemical Product Sales Center. Ammonium chloride, sodium oxalate, analyte pure, Xilong Technology Co., LTD; ammonia, analytically pure, Shanghai Suyi Chemical Reagent Co., LTD; calcium acetate, analytically pure, Tianjin Kemi Ou Chemical Reagent Co., LTD DTPA, EDTA-2Na and NTA were obtained in high purity (99.9%) from Chengdu Kelong chemical reagent factory. Barium sulfate powder (purity: 99%) was obtained from Tianjin Beichen Fangzheng, and barium sulfate scale was collected from the Changqing oilfield Ji Yuan Oil Zone gathering pipeline. The instruments used in this study included a Nicolet IS 50R Fourier transform infrared spectrophotometer (Nicolet, USA), Varian 500 MHz high-resolution NMR instrument (Varian in American). SU8000 scanning electron microscope (Hitachi High Technologies Ltd, Japan), RE-2000B rotary evaporator (Shanghai Yarong Biochemical Instrument Factory), DF-101S heat-collecting constant temperature magnetic stirrer (Gongyi Zihua Instrument Co., Ltd), FA2004 electronic balance (Shanghai Anting Electronic Instrument Factory), PHS-3c pH meter (Shanghai Leici Instrument Co., Ltd), and Materials Studio 5.0 molecular simulation software.

2.2 Experimental and characterization methods

2.2.1 Preparation of DTPA-5Na. (1) 1 mole of chloroacetic acid, 0.5 moles of sodium carbonate, 0.2 moles of diethylenetriamine, and 1.05 moles of sodium hydroxide were individually weighed. (2) Solutions of chloroacetic acid (mass concentration 56%), sodium carbonate (mass concentration 40%), and sodium hydroxide (mass concentration 40%) were prepared. (3) With the reaction temperature controlled at 5–15 °C, chloroacetic acid was added to a three-neck flask. Sodium carbonate and diethylenetriamine were subsequently added gradually and at a uniform and slow rate through a dropping funnel. Then, sodium hydroxide was slowly dripped to adjust the pH of the solution. (4) The temperature was raised to a specific level and maintained for a predetermined time. Throughout the reaction, the pH of the system was meticulously controlled. (5) After complete reaction, the resulting liquid was subjected to rotary evaporation to remove water. The residue was washed repeatedly with anhydrous ethanol, followed by rotary evaporation 2–3 times. This process yielded a pale yellow crystal, which was taken out, dried, and crushed to obtain DTPA-5Na. The reaction flow chart is shown in Fig. 1. The reaction process is illustrated in Fig. 2.

2.2.2 Determination of chelation value. Weigh 1.5 g of sample (precise to 0.01 g) and place it in a conical flask with 30 ml of deionized water. Add a sodium hydroxide solution to adjust the pH of the solution to 10. Add 15 ml of ammonium–chloride buffer solution with a pH of 10, and then slowly drip in 1 ml of oxalic acid sodium indicator (concentration 3%). Titrate the solution with a calcium acetate standard solution with a concentration of 0.1 mol L^{-1}. The endpoint is reached when the solution becomes turbid and does not disappear. Record the amount of calcium acetate consumed.[16] The chelation value formula is shown in formula (1):

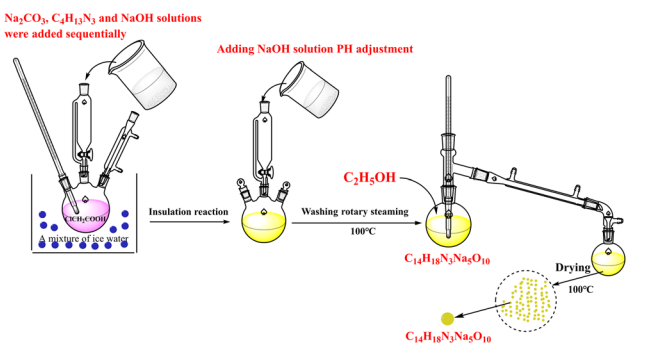

Fig. 1 Synthesis process of DTPA-5Na.

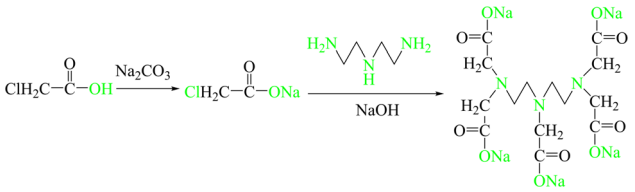

Fig. 2 Synthesis route of DTPA-5Na.

$$Y = \frac{100CV}{M} \quad (1)$$

where "Y" represents chelation value in mg $CaCO_3$ per g; "100" represents the amount of $CaCO_3$ equivalent to 1 ml of 1 mol L^{-1} calcium acetate solution in mg; "C" represents the concentration of calcium acetate solution in mol L; "V" represents the volume of consumed calcium acetate solution in ml.

2.2.3 Structural characterization of DTPA-5Na. The product was characterized using a Nicolet IS 50R spectrophotometer with a scanning frequency of 32 times, a resolution of 4 cm^{-1}, and a scanning range of 4000–400 cm^{-1}. The products were characterized by a Varian 500 MHz high-resolution NMR instrument with 16 scans using D_2O as solvent. The crystal morphology before and after the addition of DTPA-5Na was characterized by SU8000 scanning electron microscope.

2.2.4 Testing of the descaling performance. A solution with a certain mass concentration of chelating agent was prepared by adding the chelating agent into deionized water. A 100 ml aliquot of chelating agent solution was poured into a conical flask, and 1 g $BaSO_4$ scale (or barium sulfate powder) was added. The mixture was then reacted at a constant temperature water bath at 80 °C for 24 hours. After the reaction was completed, the mixture was filtered through dried filter paper, and the filter paper was weighed after being placed in a 100 °C oven for 8 hours. The scale removal rate formula is shown in formula (2), and the corrosion rate formula is shown in formula (3):

$$W = \frac{(1 + M_1 + M_2)}{1} \quad (2)$$

$$V = M \times 1 \quad (3)$$

where: "W" scale dissolution rate, %; "1" mass of $BaSO_4$, g; "M_1" weight of drying filter paper, g; "M_2" weight of filter paper dried after filtration, g; "V" dissolution amount, g.

2.3 Molecular dynamics simulation of chelation performance of DTPA-5Na

2.3.1 Creation of $BaSO_4$ crystal cell model. The crystal structure of baryte was directly imported from the Materials Studio software database. According to the literature, the primary growth surfaces for $BaSO_4$ are the (001), (100), (120), and (210) surfaces.[20–22] To model these surfaces, the cleave surface function in the Build Surface tool was utilized to cut the baryte crystal along the (001), (100), (120), and (210) surfaces within the original unit cell. The resulting crystal models were then expanded to the following respective sizes using the Super Cell function in the Build Symmetry tool: 71.072 × 43.664 × 20.722 $Å^3$, 65.496 × 64.377 × 28.212 $Å^3$, 57.224 × 55.762 × 9.699 $Å^3$, and 57.224 × 56.297 × 9.646 $Å^3$. Notably, the (001) surface contains 4608 atoms, the (100) surface contains 7776 atoms, the (120) surface contains 1728 atoms, and the (210) surface contains 2304 atoms, as depicted in Fig. 3.

2.3.2 Construction of DTPA-5Na model. Using the 3D atomistic document, a molecular model of DTPA-5Na was constructed with reference to its structural formula. Optimization was carried out from three aspects: energy, geometry and dynamics by the Forcite calculation module. This process aimed to refine the model and bring it closer to the actual material structure. By utilizing the smart algorithm with a step count of 2000, and employing the Compass force field, the spatial optimization of the model was accomplished, resulting in the energy-minimized conformation. Forcefield-assigned charges were used, and the DTPA-5Na model obtained is shown in Fig. 4.

2.3.3 Simulation of the interaction energy between DTPA-5Na and $BaSO_4$. Based on the surface model of $BaSO_4$ constructed in Section 1.3.1, a vacuum layer with a thickness of 40 Å was added. Next, the DTPA-5Na molecule was manually placed at the center of the $BaSO_4$ surface, and the COMPASS force field was employed the Badersen temperature control method was selected with a step length of 1 fs and a temperature of 80 °C (353 K). The NVT canonical ensemble was used with a step length of 500 ps, and the structure was output every 5 ps. The

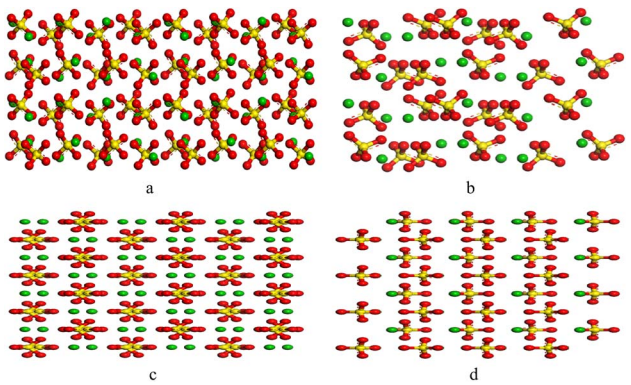

Fig. 3 Surface model of barium sulfate crystal. (a) (210) surface. (b) (120) surface. (c) (100) surface. (d) (111) surface.

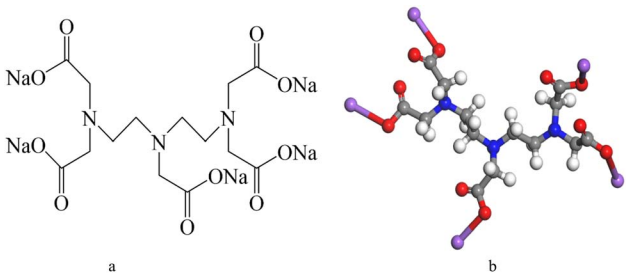

Fig. 4 Structure model of DTPA-5Na. (a) Molecular structural formula of DPTA-5Na. (b) Molecular model of DPTA-5Na.

charge was assigned using the force field method, and the electrostatic interaction was calculated using Ewald, the van der Waals force was calculated using atom based, and the cutoff distance was set to 9 Å, molecular dynamics simulations were carried out, and the models at 0 ps and 500 ps for various crystal surfaces are shown in Fig. 5.

2.3.4 Radial distribution function of adsorbed atoms in DTPA-5Na. Upon opening the trajectory file after energy calculations, the "O" and "N" atoms in the center of the DTPA-5Na molecule, as well as those on the two sides of its amino and carboxyl groups, were selected and labeled as O1, O2, N1, and N2 as shown in Fig. 6. In the Forcite Analysis module, the radial distribution function was selected, and the frame number was set from the first to the last frame. The cutoff value was set to 20 Å, and the interval was set to 0.02 Å. Radial distribution functions were then calculated between O1, O2, N1, N2 and the various crystal faces of $BaSO_4$.

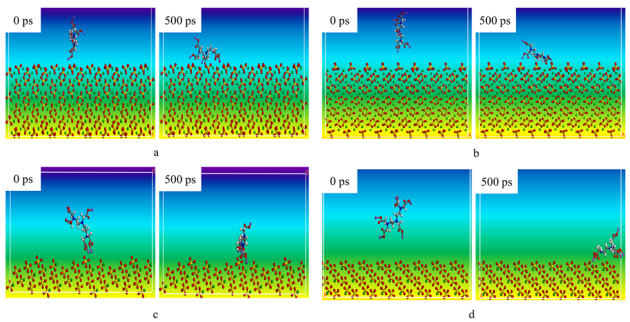

Fig. 5 Simulation of the interaction of configuration between crystal surfaces of $BaSO_4$ and DTPA-5Na. (a) Simulation of the interaction configuration between the (001) surface of BaSO4 and DTPA-5Na. (b) Simulation of the interaction configuration between the (100) surface of BaSO4 and DTPA-5Na. (c) Simulation of the interaction configuration between the (120) surface of BaSO4 and DTPA-5Na. (d) Simulation of the interaction configuration between the (210) surface of BaSO4 and DTPA-5Na.

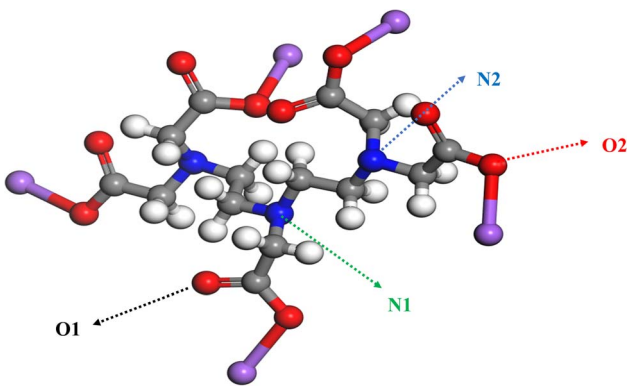

Fig. 6 Mark the adsorption atoms in the structure of DTPA-5Na.

3 Results and discussion

3.1 Synthesis and characterization of DTPA-5Na

3.1.1 Optimization of synthesis conditions for DTPA-5Na. The monomer ratio, system pH, reaction temperature, and reaction time are closely related to the chelation performance of DTPA-5Na and have a significant impact on its chelation ability. To further optimize the synthesis conditions of DTPA-5Na, an orthogonal 3-level 4-factor experimental design was adopted, as shown in Table 1. DTPA-5Na was synthesized using different schemes, and its chelation value (Y) was measured according to the chelation value measurement method in Section 1.3.1. Y was used as the evaluation criterion, and a larger Y indicates better chelation performance of DTPA-5Na. The results of the orthogonal experiment are shown in Table 2. Based on the results in Table 2, it was found that the molar ratio of the monomers had the greatest influence on the chelation performance of DTPA-5Na. The optimal conditions for the synthesis of DTPA-5Na are: $ClCH_2COOH : Na_2CO_3 : NaOH$: DETA ratio of 5.00 : 2.50 : 5.25 : 1.00, a system pH of 11.5, a reaction temperature of 50 °C, and a reaction time of 6 hours.

3.1.2 Structural characterization of DTPA-5Na. Fig. 7 shows the Fourier transform infrared spectrum of DTPA-5Na. The peak at 1621 cm^{-1} corresponds to the stretching vibration of the carboxyl group C=O, while the peak at 1103 cm^{-1} corresponds to the stretching vibration of the C–O bond. The peak at 2900 cm^{-1} corresponds to the stretching vibration of $-CH_2$, and the peak at 1338 cm^{-1} corresponds to the stretching vibration of the amine group C–N. The peaks at 3476 cm^{-1} and 668 cm^{-1} correspond to the stretching vibration and out-of-surface bending vibration of the –OH group in alcohols, respectively, which can be attributed to residual impurities from the anhydrous ethanol washing step. Furthermore, there was no observed carboxylate O–H stretching vibration absorption peak centered at 3000 cm^{-1} within the 2500–3400 cm^{-1} range, nor was there an absorption peak of the COOH bending vibration at 1395–1440 cm^{-1}. These findings indicate that COOH was not present in the synthesized product and that the monomer reaction fully took place. The results of the infrared spectrum

Table 1 Horizontal table of orthogonal experimental factors

	a	b	c	d
Level	$ClCH_2COOH/Na_2CO_3/NaOH$/DETA (molar ratio)	System pH	Reaction temperature (°C)	Reaction temperature (°C)
1	4.50 : 2.00 : 5.00 : 1.00	10.5	30	6
2	5.00 : 2.50 : 5.25 : 1.00	11.5	40	7
3	5.50 : 3.00 : 5.50 : 1.00	12.5	50	8

Table 2 Orthogonal experiment results

Experiment number	a	b	c	d	*Y*
1	a1	b1	c1	d1	32.5
2	a1	b2	c2	d2	41.8
3	a1	b3	c3	d3	30.7
4	a2	b1	c2	d3	62.9
5	a2	b2	c3	d1	76.8
6	a2	b3	c1	d2	56.8
7	a3	b1	c3	d2	46.4
8	a3	b2	c1	d3	50.6
9	a3	b3	c2	d1	45.2
K1	35.0	47.3	46.6	51.5	
K2	65.5	56.4	50.0	48.3	
K3	47.4	44.2	51.3	48.1	
R	30.5	12.2	4.7	3.4	

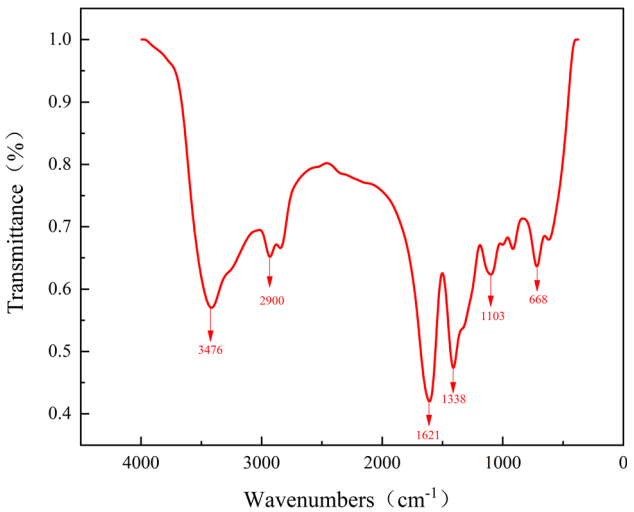

Fig. 7 Infrared spectra of DTPA-5Na.

tests demonstrate that all characteristic functional groups of DTPA-5Na are present within the synthesized product.

The proton nuclear magnetic resonance (^{1}H-NMR) spectrum of DTPA-5Na is shown in Fig. 8. In this spectrum, the chemical shifts are as follows: at $\delta = 4.79$, there is a solvent peak corresponding to D_2O; at $\delta = 3.06$, there is a peak corresponding to the methylene protons connected to the amino and carboxyl groups at both ends; at $\delta = 3.01$, there is a peak corresponding to the methylene protons connected to the central amino and carboxyl groups; at $\delta = 2.55$, there is a peak corresponding to the methylene protons connected to the amino groups at both ends; and at $\delta = 2.51$, there is a peak corresponding to the methylene protons connected to the central amino group. From the above analysis, it can be concluded that the synthesized product contains all the characteristic hydrogen atoms of DTPA-5Na.

3.2 Crystal morphology

Three equal parts of $BaSO_4$ were weighed. The first part was placed into a conical flask containing 100 ml of deionized water, the second part was placed into a conical flask containing

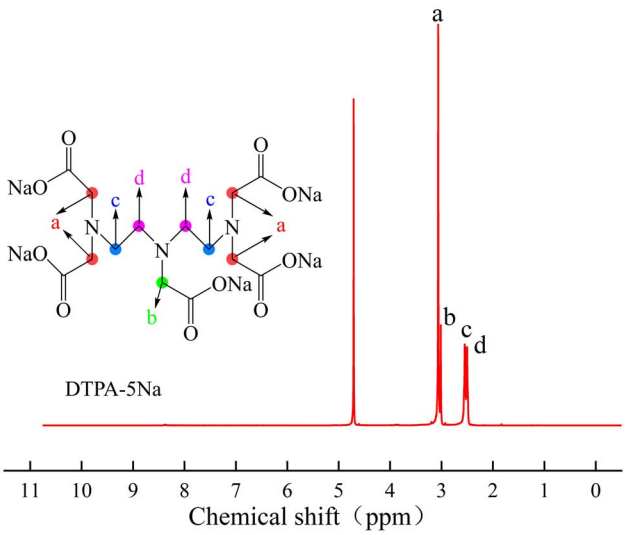

Fig. 8 Proton nuclear magnetic resonance spectrum of DTPA-5Na.

100 ml of a solution with the same pH as the working condition of DTPA-5Na, and the third part was placed into a conical flask containing 100 ml of DTPA-5Na solution. The conical flasks were then placed in a thermostatic water bath at 80 °C and allowed to react for 24 hours. After removal, they were dried. The crystal morphology of $BaSO_4$ was characterized using a SU8000 scanning electron microscope. As shown in Fig. 9a, the $BaSO_4$ crystals in deionized water had a smooth and irregular crystalline form. In this form, $BaSO_4$ was hard and strongly adhered, facilitating adsorption and accumulation. Based on Fig. 9b, $BaSO_4$ crystals placed in a water solution with the same working pH conditions as the DTPA-5Na solution exhibited a similar morphology to Fig. 9a. Both showed smooth and irregular crystalline structures, indicating that $BaSO_4$ retained its hardness and strong adhesion properties, facilitating adsorption and deposition. Fig. 9c revealed that the $BaSO_4$ crystals in the DTPA-5Na solution had a rough and porous granulated crystalline form. These irregular crystals were easily washed away by formation fluids and were difficult to adsorb and accumulate, possibly due to the introduction of DTPA-5Na into the $BaSO_4$ crystal lattice, causing lattice dislocations and deformations, resulting in a change in the crystal structure and

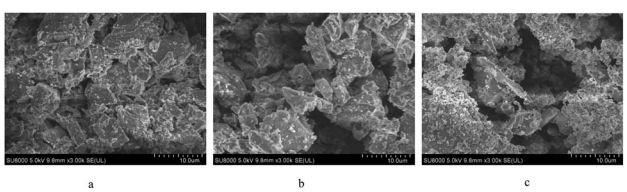

Fig. 9 Scanning electron micrograph of crystallized $BaSO_4$. (a) Morphological characterization of blank $BaSO_4$ crystal specimens (×3000). (b) Morphological characterization of $BaSO_4$ crystals after immersion under identical pH conditions (×3000). (c) Morphological characterization of $BaSO_4$ crystals after reaction with DTPA-5Na (×3000).

a decrease in density, making $BaSO_4$ more prone to dispersion in the solvent.

3.3 Evaluation of DTPA-5Na scale dissolving performance

According to the 2.2.4 Testing of the descaling performance, a comparative study of the efficacy of DTPA-5Na *versus* several commonly used amino carboxylic acid chelating agents for the removal of $BaSO_4$ scale was conducted while adjusting the solution's working pH conditions. As shown in Fig. 10a, DTPA-5Na demonstrated better scale dissolution than EDTA-2Na and NTA, attributed to DTPA-5Na's higher number of coordination atoms (8 coordination atoms from 3 amino and 5 carboxylate groups) compared to EDTA-2Na (6 coordination atoms from 2 amino and 4 carboxylate groups) and NTA (4 coordination atoms from 1 amino and 3 carboxylate groups), leading to stronger chelating ability[23] with Ba^{2+}. Compared to DTPA, DTPA-5Na exhibited a higher scale dissolution rate, possibly due to its stronger salt effect.[23] According to the scale dissolution curve at different DTPA-5Na concentrations, the dissolution rate increased first, then decreased with increasing DTPA-5Na concentration, reaching the maximum at 15% concentration. This is because at low concentrations, the increase in DTPA-5Na concentration promotes the right shift of the equilibrium between Ba^{2+} + $DTPA^{5-}$ → Ba-$DTPA^{3-}$, leading to an increase in dissolution rate. However, when the concentration of DTPA-5Na becomes too high, the chelating agent molecules tend to adsorb on the surface of $BaSO_4$, resulting in steric hindrance.[24] This weakens the chelation effect and consequently decreases the dissolution rate. Therefore, increasing the amount of DTPA-5Na does not indefinitely enhance the dissolution capacity.[25] As shown in Fig. 10b, significant changes in the morphology of $BaSO_4$ scale were observed before and after adding DTPA-5Na, likely due to DTPA-5Na diffusing to the $BaSO_4$ surface, forming complexes, and then dispersing into the solution.

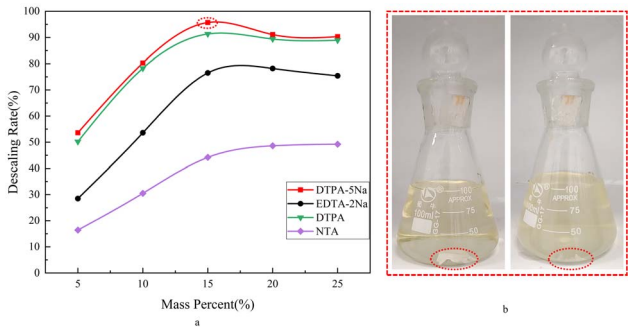

Fig. 10 Evaluation of DTPA-5Na scale dissolving performance. (a) Dissolving effect of various chelating agents at different concentrations. (b) Morphological changes of $BaSO_4$ scale before and after reaction with DTPA-5Na (15% mass percent).

3.4 Analysis of the interaction between DTPA-5Na and $BaSO_4$

The interaction energy between different molecules is used to determine the strength and stability of the intermolecular interactions within the reaction system. If the interaction energy is negative, it indicates that the adsorption process can release energy and the adsorption system is more stable, making the adsorption easier to occur. Conversely, if the interaction energy is positive, it indicates that the adsorption process requires energy absorption, making the adsorption more difficult to occur.[26–29] The magnitude of the negative interaction energy reflects the strength of the adsorption, with a larger negative value indicating a stronger adsorption. Energy analysis was performed on the DTPA-5Na and $BaSO_4$ models after dynamic simulation, and the last ten frames of the simulation were used to analyze the adsorption configurations. The calculation formula for the interaction energy between DTPA-5Na and the $BaSO_4$ crystals on each surface is shown in formula (4):

$$E_{\text{interact}} = E_{\text{total}} - E_{\text{DTPA-5Na}} - E_{\text{surface}} \quad (4)$$

where: E_{interact} is the energy released after the interaction between $BaSO_4$ crystal surfaces and DTPA-5Na binding system, kcal mol^{-1}. E_{total} is the total energy of the bonding system of $BaSO_4$ crystal surface and DTPA-5Na, kcal mol^{-1}. $E_{\text{DTPA-5Na}}$ is the single point energy of DTPA-5Na molecules in the binding system, kcal mol; E_{surface} is the single point energy of $BaSO_4$ cell in the binding system (because its surface is fixed, its energy is 0).

As shown in Table 3, the interaction energy between DTPA-5Na and different crystal planes of $BaSO_4$ is negative, indicating that they have a certain adsorption capacity and DTPA-5Na is easily adsorbed on the surface of $BaSO_4$, which impedes the accumulation of Ba^{2+} on the surface of $BaSO_4$, making it difficult for the crystal to grow. The magnitude of the interaction energy between DTPA-5Na and the various crystal planes of $BaSO_4$ is not uniform, indicating that the strength of the adsorption varies depending on the growth crystal plane. Based on the sorting of the interaction energy between the two, the strength of the adsorption of DTPA-5Na on the various crystal surfaces of $BaSO_4$ is as follows: (120) surface > (001) surface > (100) surface > (210) surface.

Table 3 Interaction energy between $BaSO_4$ crystal surface and DTPA-5Na system

Surface	E_{total} kcal mol^{-1}	$E_{\text{DTPA-5Na}}$ kcal mol^{-1}	E_{surface} kcal mol^{-1}	E_{interact} kcal mol^{-1}
(001)	−122.82	129.70	0	−252.52
(100)	−47.59	182.25	0	−229.84
(120)	−157.57	136.78	0	−294.35
(210)	2.29	155.43	0	−153.14

3.5 Radial distribution of adsorbed atoms in DTPA-5Na

The radial distribution function (RDF) is used to represent the distance distribution between a specific atom (or molecule) and its surrounding atoms (or molecules).[30] Therefore, RDF is commonly used to reflect the correlation of electrons and the orderliness of matter. The RDF can be expressed by $g(r,r')$, where $g(r,r')$ predominantly reflects the distance between atoms and the packing state of atoms when $|r - r'|$ is relatively small, when $|r - r'|$ is large, the probability of finding particles within a given distance almost no longer changes, so $g(r,r')$ gradually becomes flat and ultimately tends to a constant value.[31] Radial Distribution Functions (RDF) of O1, O2, N1, and N2 in DTPA-5Na with different surfaces of $BaSO_4$ are shown in Fig. 10.

As shown in Fig. 11a, there are significant differences in the first peak radius and peak width among the four curves, indicating that the O1 and O2 atoms of DTPA-5Na have a shorter interaction radius and closer contact with $BaSO_4$ compared to N1 and N2 atoms. Specifically, the first peak position of O1 atom is 2.86 Å with a frequency of 83.56%, and that of O2 atom is 2.79 Å with a frequency of 11.68%. Therefore, it can be concluded that both carboxyl O1 and O2 atoms of DTPA-5Na possess strong adsorption on $BaSO_4$ (001) surface, with O2 slightly stronger than O1. Similarly, Fig. 11b and c show that the O1 and O2 atoms have a shorter interaction radius and closer contact with $BaSO_4$ (100) and (120) surfaces, respectively. The first peak position of O1 atom on (100) surface is 3.13 Å with a frequency of 49.33%, and that of O2 atom is 2.93 Å with a frequency of 38.15%; while on (120) surface, the first peak position of O1 atom is 2.61 Å with a frequency of 40.95%, and that of O2 atom is 2.55 Å with a frequency of 18.02%. Therefore, it can be concluded that both carboxyl O1 and O2 atoms of DTPA-5Na possess strong adsorption on $BaSO_4$ (100) and (120) surfaces, with O2 slightly stronger than O1. Regarding the adsorption on $BaSO_4$ (210) surface, Fig. 11d shows that the central amino N2 atom of DTPA-5Na possesses the dominant role, as evidenced by its shorter interaction radius and closer contact with $BaSO_4$. Specifically, the first peak position of N2 atom on (210) surface is 6.86 Å with a frequency of 14.02%.

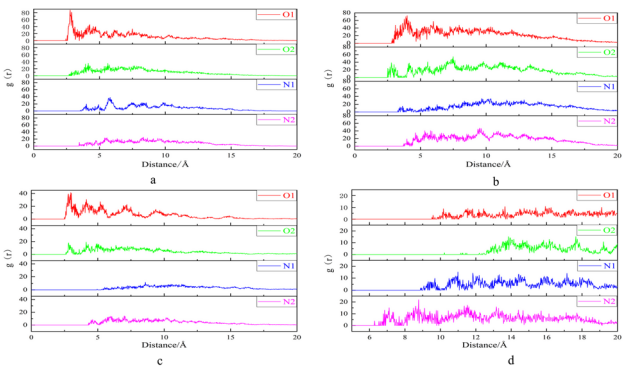

Fig. 11 Radial distribution function plots of O1, O2, N1, and N2 in DTPA-5Na and $BaSO_4$ surfaces. (a) (001) surface. (b) (100) surface. (c) (120) surface. (d) (210) surface.

In summary, according to the predicted bonding distances of DTPA-5Na on different crystal surfaces of $BaSO_4$, the dynamic adsorption capacity is ranked as (120) surface > (001) surface > (100) surface > (210) surface. Among them, the carboxyl O1 and O2 atoms play a major role on (001), (100) and (120) surfaces, with O2 having the shortest bonding distance and the strongest dynamic adsorption capacity, mainly for adsorption purposes; while O1 has a higher frequency and greater adsorption stability, mainly for chelating purposes. On (210) surface, the central amino N2 atom plays a main role, which has a longer bonding distance. Therefore, the adsorption of O atoms is stronger than that of N atoms in the structure of DTPA-5Na.

4 Conclusions

(1) By optimizing the synthesis conditions through orthogonal experiments, the molar ratio of chloroacetic acid, sodium carbonate, sodium hydroxide, and diethylenetriamine was set at 5.00 : 2.50 : 5.25 : 1.00, the reaction endpoint pH was 11.5, and the reaction was held at 50 °C for 6 hours. The resulting product exhibited good chelation performance, with a chelation value of 76.8 mg $CaCO_3$·per g.

(2) Based on the macro-scale descaling morphology of DTPA-5Na, chelation and solubilization as well as peeling and dispersion are considered as the mechanisms by which DTPA-5Na removes scale, while the micro-scale descaling morphology suggests that the mechanism of DTPA-5Na in removing scale is induced lattice distortion.

(3) Evaluation of the synthesized DTPA-5Na was carried out through a descaling experiment, which demonstrated that, with an increase in the amount of DTPA-5Na, the descaling rate initially increased and then decreased. At a concentration of 15%, the descaling rate reached 95.7%, with a dissolution amount of 0.957 g.

(4) Molecular dynamics simulations showed that the adsorption strength of DTPA-5Na varied on different growth surfaces of $BaSO_4$, with the (120) surface > (001) surface > (100) surface > (210) surface. Through radial functions calculation of DTPA-5Na's functional groups, it was found that the carboxyl atoms O1 and O2 played the main role in the (001), (100), and (120) surfaces, with O2 having the shortest bond distance and the strongest dynamic adsorption ability, mainly for adsorption; O1 had a high frequency and greater adsorption stability, mainly for chelation. On the (210) surface, the amino atom N2 played the main role, with a longer bond distance than the "O" atoms in the DTPA-5Na structure, suggesting that the adsorption ability of the "O" atoms was stronger than that of the "N" atoms.

Author contributions

Chao Ma, proposed the ideas, steps and details of the experiment, most of the experiments were done by Xin Liu, C. W., S. T. G., X. Y. H., where Xin Liu was instrumental in the proper conduct of the experiments and wrote the article together with Chao Ma, contributed equally to this work and should be

considered co-first authors, and all the authors analyzed the data, discussed the conclusions.

Conflicts of interest

The authors declare that there are no competing interests regarding the publication of this article.

Acknowledgements

We acknowledge the Foreign Experts Bureau of the Ministry of Science and Technology for the funding of the Key support program project of Foreign Experts – Surface modified nano-silica/thermosensitive polymer composites development and application in unconventional oil and gas stimulation fluids (wgxz2022057).

References

1 A. Sun, J. He, L. Fei, L. Wang, L. Qiang and M. Fang, Extrusion system of barium strontium anti-scale agent in western oilfield of South China Sea, *Sci. Tech. Eng.*, 2017, **17**(18), 198–202.

2 H. Li and J. Zhang, Progress in oilfield anti scaling technology and its application, *Chem. Ind. Eng. Technol.*, 2012, **33**(04), 40–43.

3 L. Xuejiao, *Research on the Factors Influencing Barium Sulfate Scaling and Chemical Scale Inhibition Experiments*, Southwest Petroleum University, 2015.

4 W. Yang, Y. Wang, C. Fu, *et al.*, *Experimental Investigation of the Minimum Inhibitor Concentration in Porous Media[C]//SPE International Oilfield Scale Conference and Exhibition*, OnePetro, 2020.

5 Y. Wang, X. Li and J. Lu, Physicochemical modeling of barium and sulfate transport in porous media and its application in seawater-breakthrough monitoring, *SPE J.*, 2021, **26**(06), 3855–3876.

6 F. Lin, F. You, S. Wang and P. Yang, Anti-barium sulfate sedimentation technology of weighted drilling fluid, *Drill. Fluid Completion Fluid*, 2015, **32**(03), 27–29.

7 Y. Dong, D. Chang, L. Hu, *et al.*, Research and Application of Complex Method for Removing Barium Sulfate from Oilfield, *Drill. Fluid Completion Fluid*, 2017, **34**(03), 122–126.

8 Z. Tariq, M. S. Kamal, M. Mahmoud, *et al.*, Self-destructive barite filter cake in water-based and oil-based drilling fluids, *J. Pet. Sci. Eng.*, 2021, **197**, 107963.

9 H. Li, L. Ran, T. Liu, *et al.*, Study on the Effect of Scale Inhibitors on the Kinetic Parameters of Barium Sulfate Crystallization, *J. Southwest Pet. Univ.*, 2022, **44**(05), 175–184.

10 L. Cheng, Y. Liang, Y. Li, *et al.*, Research and application of barium sulfate strontium scale control technology in the west oilfield of South China Sea, *Drill. Prod. Technol.*, 2020, **43**(01), 61–64.

11 H. Sun, Y. Chen and H. Qian, Oilfield descaling technology research progress, *J. Chem. Reagents*, 2012, (11), 991–994, DOI: 10.13822/j.cnki.hxsj.2012.11.026.

12 S. Wu, L. Cheng, X. Wan, *et al.*, Evaluation of an efficient and economical barium strontium scale remover system for offshore oil wells and research on its scale removal process, *China Surfactant Deterg. Cosmet.*, 2022, **52**(10), 1062–1071.

13 F. M. Alissa, N. W. Aljuryyed, S. A. Balharth, *et al.*, *Calcium Sulfate Scale Dissolution Efficiency by Various Chemicals Additives[C]//SPE International Conference and Exhibition on Formation Damage Control*, OnePetro, 2022.

14 M. Fu, Experimental study on the dissolution of barium sulfate scale with DTPA, *Drill. Prod. Technol.*, 1999, (01), 61–62.

15 Ai Fei, Improvement of DTPA pentasodium salt synthesis process, *Yunnan Chem. Ind.*, 2019, **46**(05), 93–95.

16 Z. Lin, DTPA chelating agent and its manufacturing, *Pap. Papermaking*, 2005, (03), 63–64.

17 J. Wang, Study on the synthesis process of sodium diethylenetriamine pentaacetate chelating agent, *Leather Chem. Ind.*, 1998, (04), 26–27.

18 Y. Xu, Z. Chen, Y. Gao, *et al.*, Synthesis of DTPA and its application in oxygen bleaching, *Print. Dyeing*, 2021, **47**(10), 16–20.

19 C. Zhuang and H. Yue, Zhang Huijun Application of Molecular Simulation Methods and Simulation Software Ma materials Studio in Polymer Materials, *Plastics*, 2010, **39**(4), 81–84.

20 X. Geng, R. D. Sosa, M. A. Reynolds, *et al.*, Alginate as a green inhibitor of barite nucleation and crystal growth, *Mol. Syst. Des. Eng.*, 2021, **6**(7), 508–519.

21 A. G. Stack, Molecular dynamics simulations of solvation and Kink Site formation at the {001} Barite – Water interface, *J. Phys. Chem. C*, 2009, **113**(6), 2104–2110.

22 R. D. Sosa, X. Geng, A. Agarwal, *et al.*, Acidic polysaccharides as green alternatives for barite scale dissolution, *ACS Appl. Mater. Interfaces*, 2020, **12**(49), 55434–55443.

23 B. Xu, *Research on Chemical Cleaning of Barium Strontium Sulfate Scale*, Southwest Petroleum University, 2016.

24 T. Almubarak, J. H. Ng, and H. Nasr-El-Din, Oilfield Scale Removal by Chelating Agents: An Aminopolycarboxylic Acids Review, *Paper presented at the SPE Western Regional Meeting*, Bakersfield, California, 2017.

25 W. Zhongjin, F. Zhou and T. Xu, Review on the mechanism of barium sulfate filter cake blockage and the decision-making technology of chelation blockage removal, *Drill. Fluid Completion Fluid*, 2020, **37**(06), 685–693.

26 Y. M. Tang, F. Zhang, Z. Y. Cao, *et al.*, Crystallization of CaCO3 in the presence of sulfate and additives: Experimental and molecular dynamics simulation studies, *J. Colloid Interface Sci.*, 2012, **377**, 430–437.

27 W. Y. Shi, C. Ding, J. L. Yan, *et al.*, Molecular dynamics simulation for interaction of PESA and acrylic copolymers with calcite crystal surfaces, *Desalination*, 2012, **291**, 8–14.

28 E. Hadicke, J. Rieger, I. U. Rau, *et al.*, Molecular dynamics simulations of the incrustation inhibition by polymeric additives, *Phys. Chem. Chem. Phys.*, 1999, **1**(17), 3891–3898.
29 F. Jones, W. R. Richmond and A. L. Rohl, Molecular modeling of phosphonate molecules onto barium sulfate terraced surfaces, *J. Phys. Chem. B*, 2006, **110**(14), 7414–7424.
30 W. Shi, F. Wang, M. Xia, *et al.*, Molecular dynamics simulation of interaction between carboxylate copolymer and calcite crystal, *Acta Chim. Sin.*, 2006, **64**(17), 1817.
31 C. Chen, W. Lei, M. Xia, *et al.*, Molecular modeling of several phosphonates onto the stepped calcite (011) surface, *Desalination*, 2013, **309**, 208–212.